


 Cite this: *RSC Adv.*, 2025, 15, 37062

# Sulfidation of magnetic CoFeAl-layered double hydroxide material as peroxymonosulfate activator for efficient degradation of norfloxacin

Xingzi Zhu, Xiaoxin Chen, Jinxin Wang, Caiyan Ge, Manli Guo, \* Yujuan Cao and Bixia Lin

A magnetic CoFeAl-layered double hydroxide (LDH) material was synthesized *via* a hydrothermal method, followed by sulfidation treatment with sodium sulfide, and the obtained S/CoFeAl-LDH nanocomposite was used as a peroxymonosulfate (PMS) activator for efficient degradation of antibiotics in water by using norfloxacin (NOR) as a model. Through sulfidation modification, the proportion of low-valent metal ions in the composites was increased. Therefore, the S/CoFeAl-LDH displayed a higher performance of NOR degradation *via* the activation of PMS than the CoFeAl-LDH. Within 6 min, 0.10 g per L S/CoFeAl-LDH and 0.20 g per L PMS could degrade 98.3% NOR (20 mg L<sup>-1</sup>). S/CoFeAl-LDH, as a heterogeneous catalyst, could efficiently activate PMS and degrade NOR in the pH range of 4–9. Since the synthesized material was a composite of magnetic CoFe<sub>2</sub>O<sub>4</sub> and LDH, it could be recycled by magnetism after the reaction. After 4 cycles, the NOR degradation rate still reached 84.3%, indicating the good stability of the catalyst. During the degradation of NOR by S/CoFeAl-LDH/PMS, both free radical pathway and non-free radical pathway played a role, among which SO<sub>4</sub><sup>•-</sup>, O<sub>2</sub><sup>•-</sup> and <sup>1</sup>O<sub>2</sub> were the main active species. The Co<sup>2+</sup> and Fe<sup>2+</sup> in the composites reacted with PMS to generate active species. The synergistic effect of metals and the reducibility of sulfur further promoted the cyclic regeneration of Co<sup>2+</sup> and Fe<sup>2+</sup>, which was conducive to the activation of PMS to generate free radicals. In addition, the intermediate products of the degradation reaction were analyzed by LC-MS, and the possible degradation paths were put forward. This study revealed that the S/CoFeAl-LDH was a heterogeneous catalyst with good application prospect, which provides a new method for removing antibiotics from water.

 Received 1st August 2025  
 Accepted 1st October 2025

DOI: 10.1039/d5ra05588a

[rsc.li/rsc-advances](https://rsc.li/rsc-advances)

## 1. Introduction

Antibiotics have excellent antibacterial properties and have been widely used in industries such as healthcare, aquaculture, and livestock and poultry farming.<sup>1,2</sup> The appropriate use of antibiotics can effectively control bacterial infections and aid in restoring health. However, the abuse of antibiotics can harm human health as well as aquatic environments and ecosystems.<sup>3</sup> Traditional wastewater treatment technologies such as physical, chemical, and biological methods have certain effectiveness in removing organic pollutants from waste water.<sup>4–6</sup> Physical adsorption can simply and conveniently remove organic pollutants from water, but it cannot degrade them into less toxic or even non-toxic substances. Additionally, chemical methods like electro dialysis can effectively separate organic pollutants from water, but they involve high operational costs. Biological processes such as bioreactors, activated sludge and microbial treatment have many positive aspects, but they also suffer from

drawbacks such as slow degradation rates, low biodegradability of dyes and the potential formation of biological sludge.

Therefore, the development of rapid, efficient, widely applicable and low-cost methods is crucial for degrading antibiotics in water.

Advanced oxidation processes (AOPs) represent a kind of water treatment technologies that employ electricity, photo-radiation, catalysts, or oxidants to generate highly reactive free radicals (primarily hydroxyl radicals <sup>•</sup>OH) for the efficient degradation of organic pollutants.<sup>5–11</sup> AOPs can decompose the vast majority of refractory organic substances (such as antibiotics, pesticides and dyes), and eventually mineralize them into CO<sub>2</sub>, H<sub>2</sub>O or small molecules.<sup>12</sup> The AOP based on peroxymonosulfate (PMS) has a good application prospect due to its strong oxidizing property, low cost, rapidity and high efficiency.<sup>13,14</sup> However, PMS itself has limited oxidative capacity and requires activation methods (*e.g.*, UV irradiation, transition metal activation, or carbon-material activation) to generate free radicals.<sup>15–18</sup>

Transition metal ions such as Co<sup>2+</sup>, Ni<sup>2+</sup>, Cu<sup>2+</sup> and Fe<sup>3+</sup> can effectively activate PMS to generate sulfate radicals (SO<sub>4</sub><sup>•-</sup>), but metal ions in homogeneous systems are difficult to reuse, which

School of Chemistry, Guangzhou Key Laboratory of Analytical Chemistry for Biomedicine, South China Normal University, Guangzhou 510006, China. E-mail: manliguo@163.com



can cause secondary pollution.<sup>19</sup> The use of heterogeneous catalyst/PMS systems can prevent the leaching of metal ions and reduce energy consumption.<sup>20</sup> Layered double hydroxide (LDH) is a type of layered materials with two-dimensional nanostructures, commonly known as hydrotalcite. LDH is primarily composed of positively charged laminates and interlayer anions, with the general formula  $[M_{1-x}^{2+}M_x^{3+}(\text{OH})_2]^{x+}[(A^{n-})_{x/n} \cdot m\text{H}_2\text{O}]$ .<sup>21</sup> Featuring tunable internal structures and exchangeable interlayer anions, LDH can be used as heterogeneous catalysts to activate PMS for removing organic pollutants in water.<sup>22,23</sup> In addition, introducing a third metal ion can modulate the electronic structure and coordination environment of the layered metals, increasing the number of reactive sites. Through the synergistic effect of the three metals, the electron transfer efficiency of LDH can be optimized, thereby enhancing the material's ability to activate PMS and improving degradation efficiency.<sup>24</sup> Li *et al.*<sup>25</sup> designed a ternary CoFeAl-LDH to catalyze PMS for the degradation of ciprofloxacin (CIP), which improved metal loading capacity and catalyst reusability. Experimental results demonstrated that the significant synergistic interaction among Co, Fe and Al effectively suppressed the formation of high-valent metal-oxo species, achieving a CIP degradation rate of 91.4% within 60 min. Zeng *et al.*<sup>26</sup> synthesized magnetic CoFeNi-LDH and applied it to activate PMS to degrade dyes. The study showed that the cyclic activation of PMS between Co(II) and Co(III) produced sulfate radical to participate in the degradation process. To further enhance the PMS activation performance of LDHs, methods such as modifying interlayer anions, using carbon materials to alter surface properties, doping with transition metals or incorporating organic compounds have been employed.<sup>27–30</sup> Notably, sulfurization treatment of a LDH can adjust the electronic structure of the catalyst, thereby improving the electron transfer ability of the catalyst.<sup>31,32</sup>

Based on the aforementioned research, in this study, a magnetic ternary CoFeAl-LDH was synthesized *via* a hydrothermal method, followed by further treatment of the LDH with sodium sulfide. The final product S/CoFeAl-LDH was used as a heterogeneous catalyst to activate PMS for the degradation of antibiotics in water, using norfloxacin (NOR) as a model. The purpose of this work is to: (1) characterize the synthesized S/CoFeAl-LDH; (2) evaluate its effect of activating PMS to degrade NOR; (3) explore the reaction mechanism of S/CoFeAl-LDH activated PMS for the degradation of NOR; (4) propose possible degradation pathways of NOR.

## 2. Experimental

### 2.1. Chemicals and reagents

All the chemicals and reagents used were of analytical grade. A detailed list of reagents is shown in Text S1 in the SI.

### 2.2. Preparation of S/CoFeAl-LDH catalyst

For the preparation of CoFeAl-LDH, 2 mmol  $\text{CoCl}_2 \cdot 6\text{H}_2\text{O}$ , 1 mmol  $\text{FeCl}_3 \cdot 6\text{H}_2\text{O}$  and 1 mmol  $\text{AlCl}_3 \cdot 6\text{H}_2\text{O}$  were dissolved in 80 mL of deionized water evenly and thoroughly to make

a mixed metal salt solution. NaOH solution was continuously added to stabilize the pH at  $10 \pm 0.2$ . Then, the mixture was transferred into a 100 mL Teflon-lined stainless steel autoclave and heated at 120 °C for 6 h. After natural cooling to room temperature, the sample was collected and washed with ethanol and deionized water for several times, and then dried at 60 °C for 24 h.

50 mg of CoFeAl-LDH was dispersed in 30 mL  $\text{Na}_2\text{S}$  solution (0.2 M) and stirred for 15 min. After filtering, it was washed with ethanol and deionized water for several times. After drying in an oven, the product S/CoFeAl-LDH was obtained. The schematic illustration of the formation of S/CoFeAl-LDH is shown in Fig. S1.

### 2.3. Characterization

The morphologies and microstructures of catalysts were examined by scanning electron microscopy (SEM, ZEISS Sigma 360, Germany) and transmission electron microscopy (TEM, FEI Talos F200X, USA). Energy-dispersive spectroscopy (EDS) was utilized to determine the elemental distributions thereon. Vibrating sample magnetometry (VSM, LakeShore 7404, USA) was used to analyze the magnetic properties of the catalysts. The crystal structures of the catalysts before and after sulfidation were determined by X-ray diffraction (XRD, Bruker D8 Advance Davinci). The elemental compositions and distributions of the catalysts before and after reaction were investigated by X-ray photoelectron spectroscopy (XPS, AXIS SUPRA).

### 2.4. Degradation experiments

Batch catalytic degradation experiments were performed in a 100 mL conical flask with a shaker speed of 150 rpm. The temperature of the degradation experiment was maintained at 25 °C. In a typical process, 5 mg catalyst and 2 mL PMS solution were added into 48 mL of NOR solution (NOR final concentration, 20 mg  $\text{L}^{-1}$ ; PMS final concentration, 0.2 g  $\text{L}^{-1}$ ). 1 mL of liquid sample was taken from the mixture at a certain time interval, quenched with methanol and filtered through a 0.22  $\mu\text{m}$  membrane prior to analysis. All experiments were conducted at least in triplicates, and the results were expressed as mean values with standard deviations.

### 2.5. Analysis methods

NOR concentrations were determined using high performance liquid chromatography (HPLC, Shimadzu LC-20 ADXR, Japan) equipped with a C18 column (Agilent Zorbax XDB-C18, USA). The detection wavelength was 280 nm, the mobile phase was composed of acetonitrile (15%) and 0.1% formic acid water (85%), and the flow rate was 1 mL  $\text{min}^{-1}$ . Intermediates generated during NOR degradation were detected by HPLC/MS. Total organic carbon (TOC) values were measured by using a TOC-L analyzer (Shimadzu). The experimental procedures for the detection of the degradation products were given in Text S2. Inductively coupled plasma mass spectrometer (ICP-MS) was used to determine the leached concentrations of copper and iron ions. The active species generated during reaction were detected by electron paramagnetic resonance spectrometer



(EPR, Bruker EMX plus-6/1, Germany). Chronoamperometry experiments were conducted on an electrochemical workstation to analyze the electrochemical performances of the catalysts.

### 3. Results and discussion

#### 3.1. Characterization

The morphologies and microstructures of CoFeAl-LDH and S/CoFeAl-LDH were characterized by SEM. In Fig. 1, CoFeAl-LDH and S/CoFeAl-LDH had nanosheet structures, and the nanosheets were closely packed together, with fine particles

covering the surface. Meanwhile, it can be observed that the surface morphology of the CoFeAl-LDH material did not change significantly after sulfidation, indicating that the sulfidation process had no significant effect on the crystal structure of CoFeAl-LDH. The TEM image (Fig. 2a) further verified the microstructure of S/CoFeAl-LDH, and the presence of LDH nanosheets could be observed in the stacked structure. Furthermore, the HR-TEM images (Fig. S2) showed that S/CoFeAl-LDH had a typical LDH crystal form. Lattice fringes with spacings of 0.15 nm, 0.23 nm, and 0.26 nm could be observed, corresponding to the (113), (015), and (012) crystal

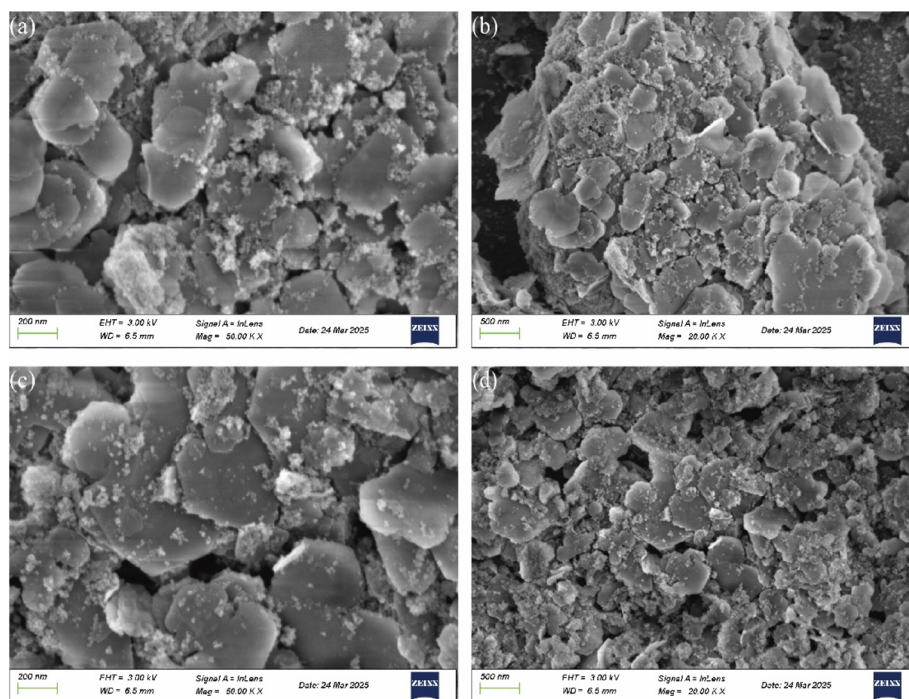


Fig. 1 SEM images of CoFeAl-LDH (a and b) and S/CoFeAl-LDH (c and d).

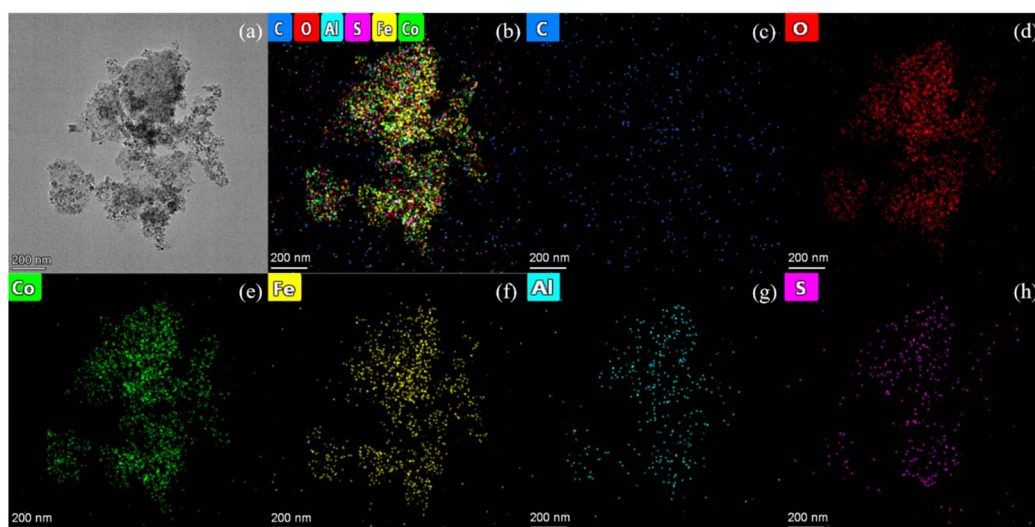


Fig. 2 TEM image of S/CoFeAl-LDH (a) and elemental mappings of S/CoFeAl-LDH of different elements (b–h).



planes of LDH, respectively.<sup>33,34</sup> Element mapping revealed the distribution of each element in S/CoFeAl-LDH. As shown in Fig. 2b–h, Co, Fe, Al, O and S were uniformly distributed in the sample. The EDS energy spectrum (Fig. S3) revealed the content of each element in the S/CoFeAl-LDH.

Fig. 3a showed the XRD patterns of CoFeAl-LDH and S/CoFeAl-LDH. The diffraction peaks at 11.6°, 23.2°, 60.2°, and 61.6° corresponded to the (003), (006), (110), and (113) crystal planes of CoFeAl-LDH (PDF #37-0630), respectively.<sup>25</sup> It indicated that the ternary CoFeAl-LDH had been successfully synthesized. The characteristic peak intensity of LDH treated with Na<sub>2</sub>S decreased obviously, indicating that some crystalline hydroxides were transformed into hydroxyl sulfides.<sup>31</sup> At the same time, S<sup>2-</sup>, SO<sub>4</sub><sup>2-</sup> and other ions generated during sulfidation enter the interlayers, altering the original interlayer spacing and weakening the diffraction peak intensity. The peaks at 30.2°, 35.6°, 43.1°, 56.9° and 62.7° matched the standard spectrum of CoFe<sub>2</sub>O<sub>4</sub> (PDF #22-1086), indicating that the prepared sample was a composite material consisting of CoFe<sub>2</sub>O<sub>4</sub> and LDH with magnetic properties.<sup>35</sup> The magnetism of the material was tested by VSM. As observed in Fig. 3b, both CoFeAl-LDH and S/CoFeAl-LDH had certain magnetic properties, and S/CoFeAl-LDH had a stronger magnetic property,

which facilitated the recovery and reuse of the catalyst after the catalytic degradation of antibiotics.

The elements and valence states on the surface of S/CoFeAl-LDH were explored by XPS. The XPS spectrum of C 1s was shown in Fig. 4a. The peaks at 284.80, 286.60 and 288.70 eV could be assigned to C–C, C=O and C–O=O, respectively.<sup>25</sup> There were two peaks at 530.12 and 532.16 eV in the O 1s spectrum (Fig. 4b), corresponding to M–OH and M–O–M respectively.<sup>36</sup> In the XPS spectrum of Co 2p (Fig. 4c), the peaks at 781.69 and 797.08 eV belonged to Co(III), while the peaks at 785.80 and 803.80 eV corresponded to Co(II).<sup>37</sup> As shown in the Fe 2p spectrum (Fig. 4d), two satellite peaks and four main peaks could be seen. The fitting peaks at 710.96 and 723.76 eV revealed the existence of Fe(II), while the peaks at 713.16 and 726.40 eV were attributed to Fe(III). The other two peaks at 716.12 and 719.92 eV were satellite peaks.<sup>33</sup> For Al 2p (Fig. 4e), the peak at 74.64 eV could be attributed to the formation of Al–O.<sup>38</sup> In the S 2p spectrum (Fig. 4f), four main peaks could be observed at 163.88, 165.18, 168.72 and 170.02 eV, which were attributed to M–S 2p<sub>3/2</sub>, M–S 2p<sub>1/2</sub>, SO<sub>x</sub> 2p<sub>3/2</sub> and SO<sub>x</sub> 2p<sub>1/2</sub>, respectively.<sup>38,39</sup> No peaks for S element was observed for the CoFeAl-LDH (Fig. S4a). The presence of Cl was detected in the CoFeAl-LDH; nevertheless, the S/CoFeAl-LDH did not show any Cl signal (Fig. S4b). These results proved that sulfate and sulfite ions replaced the Cl<sup>-</sup> between the LDH layers after sulfidation. After sulfurization treatment, metal sulfides were introduced, and sulfate and sulfite ions were also produced. The results of EDS showed that the proportion of sulfur in S/CoFeAl-LDH was only 2.28%, meaning that the content of sulfur-related species produced was relatively low. However, the introduced sulfur played a role in modulating the valence states of metals in the material. After sulfurization treatment of the LDH, the content of Co<sup>2+</sup> increased from 29.57% to 41.03%, while the content of Fe<sup>2+</sup> rose from 28.25% to 32.98% (Fig. S4c and d). This confirmed that the sulfur reduced the high-valence metal ions (Co<sup>3+</sup>/Fe<sup>3+</sup>) to low-valence states (Co<sup>2+</sup>/Fe<sup>2+</sup>). Since low-valence transition metal ions can effectively activate PMS to generate free radicals, the sulfurization treatment was beneficial for the degradation process. Additionally, after sulfidation, the binding energy of the Co 2p<sub>3/2</sub> main peak shifted from 780.02 eV to 781.69 eV, and the entire Fe 2p spectrum exhibited a positive shift of approximately 1.68–2.48 eV. This positive shift indicated a decrease in the electron density on Co and Fe atoms, which could be attributed to the formation of M–S bonds during the sulfidation process.

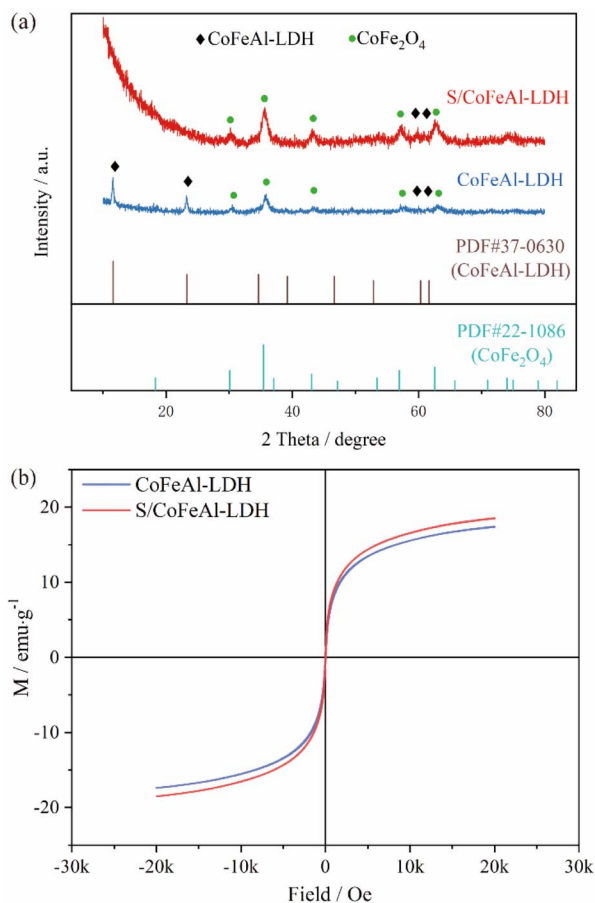


Fig. 3 XRD images (a) and hysteresis loops (b) of CoFeAl-LDH and S/CoFeAl-LDH.

### 3.2. Degradation of NOR

Fig. 5a showed the degradation efficiency of NOR in different systems. Without the addition of PMS, the removal rates of NOR by CoFeAl-LDH and S/CoFeAl-LDH were less than 5% within 6 min, which indicated that these two materials had weak adsorption effects on NOR. When only PMS was present in the system, the removal rate of NOR was approximately 55% within 6 min. The heterogeneous catalyst/PMS system demonstrated an excellent NOR removal performance. When the initial concentration of NOR was 20 mg L<sup>-1</sup>, using S/CoFeAl-LDH as the catalyst to activate PMS, 80.0% of NOR could be degraded

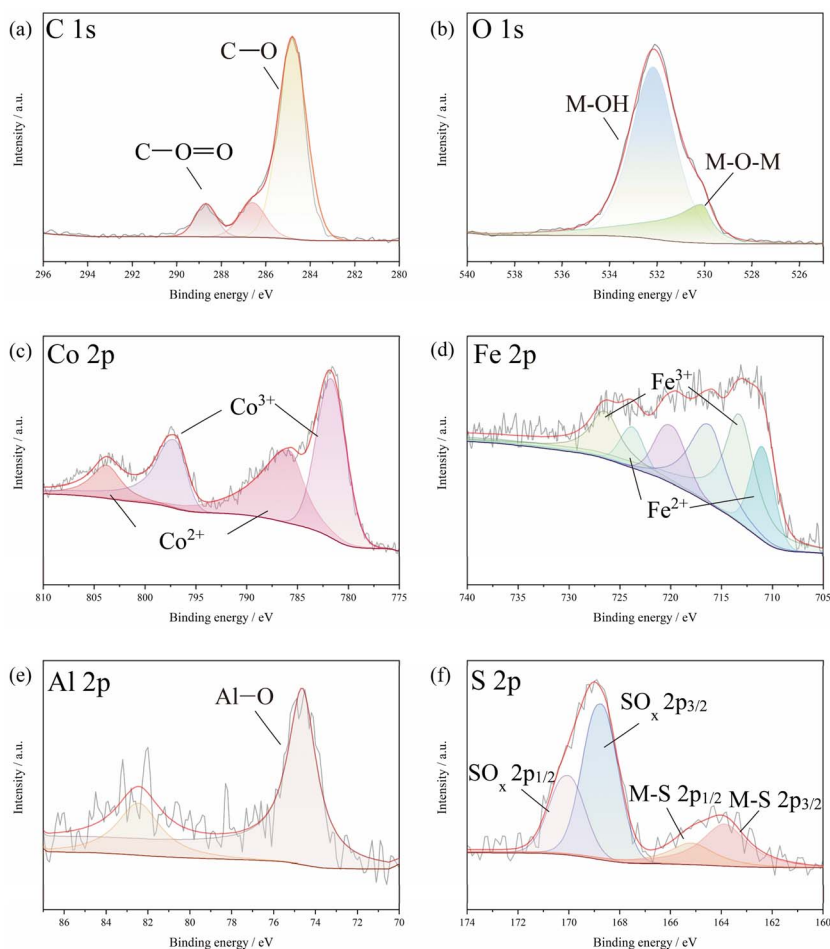


Fig. 4 XPS spectra of C 1s (a), O 1s (b), Co 2p (c), Fe 2p (d), Al 2p (e), and S 2p (f) of S/CoFeAl-LDH.

within 1 min, while the removal rate of CoFeAl-LDH/PMS was 64.1%. Within 6 min, the NOR removal rates of S/CoFeAl-LDH/PMS and CoFeAl-LDH/PMS were 98.3% and 82.9%, respectively. It could be seen that using S/CoFeAl-LDH/PMS can achieve near complete elimination of NOR, which was better than CoFeAl-LDH/PMS. In addition, when using the same concentration of CoFe<sub>2</sub>O<sub>4</sub> to activate PMS for NOR degradation, the removal rate

within 6 min was 84.3%. It proved that S/CoFeAl-LDH/PMS can remove NOR from water quickly and efficiently.

As shown in Fig. S5, the TOC removal rate gradually increased during the degradation process. The TOC removal rate rose from 45.1% at 1 min to 62.0% at 6 min. Upon further extension of the degradation time, the TOC removal rate slightly increased to 62.7% at 10 min and then remained essentially unchanged thereafter.

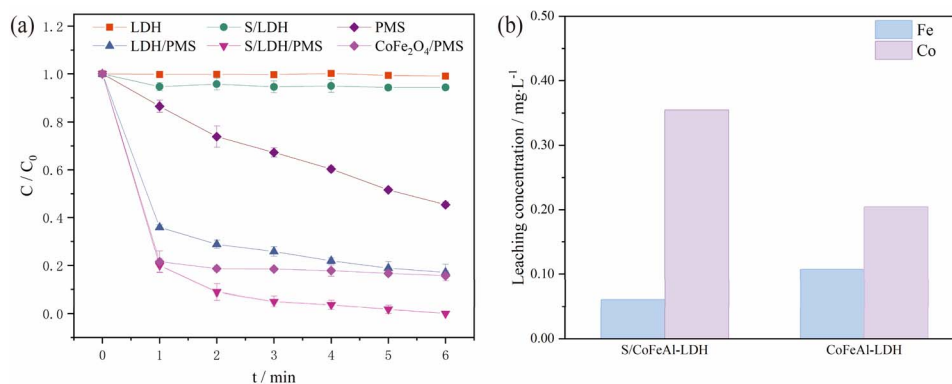


Fig. 5 Removal of NOR under different systems (a) and leaching concentration of cobalt and iron after degradation (b). Reaction conditions:  $C_{\text{catalyst}} = 0.1 \text{ g L}^{-1}$ ,  $C_{\text{PMS}} = 0.2 \text{ g L}^{-1}$ ,  $C_{\text{NOR}} = 20 \text{ mg L}^{-1}$ , initial pH = 6.8.



The leaching concentrations of transition metal ions during the reaction process were detected by ICP-MS. As shown in Fig. 5b, the leaching concentrations of Co from S/CoFeAl-LDH and CoFeAl-LDH after the reaction were  $0.35 \text{ mg L}^{-1}$  and  $0.20 \text{ mg L}^{-1}$ , respectively, while the leaching concentrations of Fe were  $0.06 \text{ mg L}^{-1}$  and  $0.11 \text{ mg L}^{-1}$ , respectively. All were below the national emission standards (GB 3838-2002,  $1.0 \text{ mg L}^{-1}$  for Co, and  $0.3 \text{ mg L}^{-1}$  for Fe). Therefore, the S/CoFeAl-LDH/PMS used in this work can effectively inhibit the leaching of metal ions and avoid secondary pollution. It represented an environmentally friendly NOR degradation method.

### 3.3. Optimizations of parameters on the degradation of NOR

**3.3.1. Effect of sodium sulfide concentration.** Previous studies had demonstrated that LDH treated with sulfidation exhibited a superior NOR degradation effect. In order to explore the differences in catalytic activity of LDHs treated with varying concentrations of  $\text{Na}_2\text{S}$ , the LDH catalyst was treated with 0.1 M, 0.2 M and 0.5 M  $\text{Na}_2\text{S}$  solutions, respectively. As shown in Fig. 6a, the catalyst treated with 0.5 M  $\text{Na}_2\text{S}$  solution exhibited the best degradation performance, indicating that treating LDH with a higher concentration of  $\text{Na}_2\text{S}$  solution can enhance the activity of the catalyst.<sup>40</sup> Therefore, the catalyst S/CoFeAl-LDH treated with 0.5 M  $\text{Na}_2\text{S}$  was selected to activate PMS to degrade NOR.

**3.3.2. Effect of sodium sulfide concentration.** Different dosages of catalysts were added to investigate their effects on the degradation of NOR (Fig. 6b). With the increase of catalyst dosage, the removal rate of NOR first increased and then slightly decreased. Among them, the highest NOR removal rate

of 98.3% within 6 min was achieved at a catalyst dosage of  $0.10 \text{ g L}^{-1}$ . At higher dosages of the catalyst ( $0.15$  and  $0.20 \text{ g L}^{-1}$ ), most NOR could be rapidly degraded within 1 min, and the removal rates at 6 min were approximately 90%. These results demonstrated that increasing the dosage of the catalyst could provide more reactive sites and generate more active species in the system. Therefore, the removal rate can be improved within a certain range. However, excessive catalysts may accumulate together during the reaction process, affecting subsequent degradation. Moreover, higher catalyst concentrations increased solution turbidity, which could weaken the transmission intensity of visible light during detection.<sup>41</sup> Therefore,  $0.10 \text{ g L}^{-1}$  of catalyst was added in the subsequent experiments.

**3.3.3. Effect of PMS dosage.** The effect of PMS dosage ( $0.05$ – $0.30 \text{ g L}^{-1}$ ) on the degradation of NOR is shown in Fig. 6c. With the increase of PMS dosage, the removal rate of NOR in the system gradually increased. When the PMS dosage was  $0.05 \text{ g L}^{-1}$ , the NOR removal rate within 6 min reached only 12.2%. As the PMS dosage increased to  $0.10$  and  $0.15 \text{ g L}^{-1}$ , the removal rates significantly improved to 48.4% and 91.9%, respectively. It demonstrated that the PMS dosage was a key factor affecting the degradation efficiency. With the increase of the PMS dosage, S/CoFeAl-LDH in the system could catalyze more PMS to produce active species, thus enabling the rapid and efficient degradation of NOR. In order to achieve a high removal rate and reduce the dosage of reagents,  $0.20 \text{ g}$  per  $\text{L}$  PMS was added in the subsequent experiments to remove NOR.

**3.3.4. Effect of initial NOR concentration.** The effect of initial NOR concentration on the degradation efficiency by S/CoFeAl-LDH/PMS is shown in Fig. 6d. With the increase of initial NOR concentration, the NOR removal rate decreased

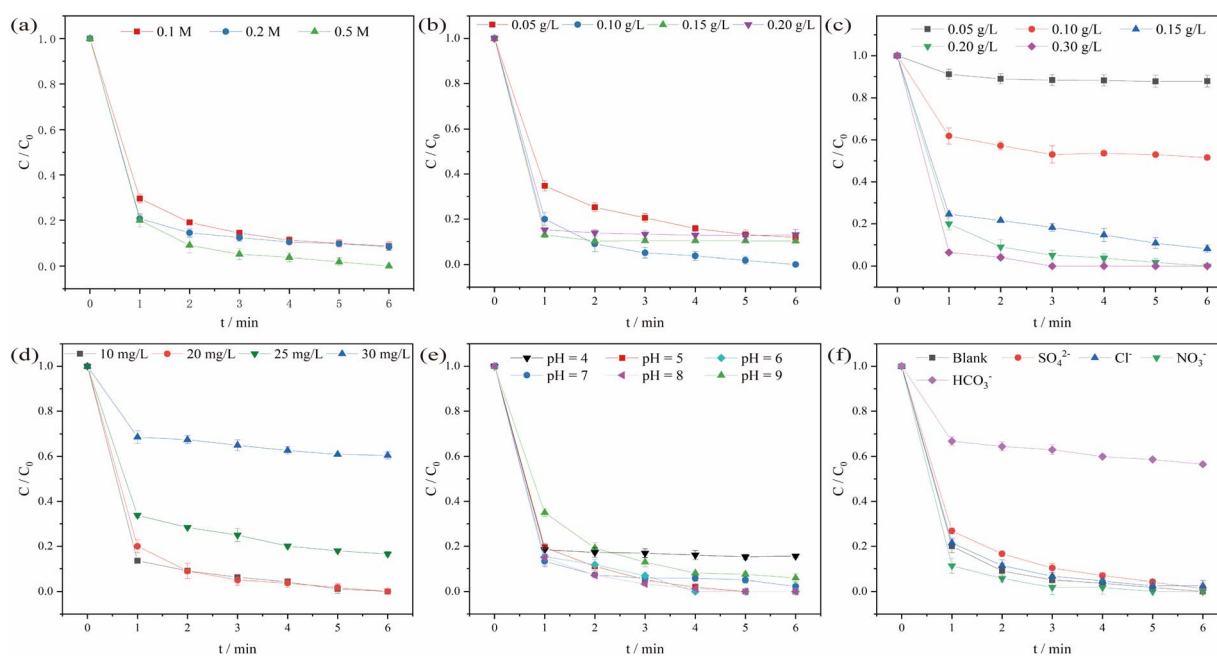


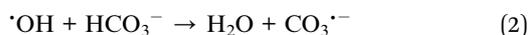
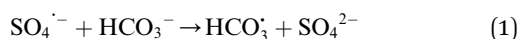
Fig. 6 Effects of different parameters on removal of NOR:  $\text{Na}_2\text{S}$  concentration during the preparation of S/CoFeAl-LDH (a), S/CoFeAl-LDH dosage (b), PMS dosage (c), initial NOR concentration (d), initial pH (e) and inorganic anions (f). Reaction conditions:  $c_{\text{catalyst}} = 0.1 \text{ g L}^{-1}$ ,  $c_{\text{PMS}} = 0.2 \text{ g L}^{-1}$ ,  $c_{\text{NOR}} = 20 \text{ mg L}^{-1}$ , initial pH = 6.8,  $c_{\text{SO}_4^{2-}} = c_{\text{Cl}^-} = c_{\text{NO}_3^-} = c_{\text{HCO}_3^-} = 5 \text{ mM}$ .



significantly. When the initial concentrations of NOR were 10 and 20 mg L<sup>-1</sup>, the NOR removal rates within 6 min were 98.9% and 98.3%, respectively. As the concentration increased to 25 and 30 mg L<sup>-1</sup>, the NOR removal rates decreased to 83.5% and 49.5%, respectively. This phenomenon occurred because the amount of catalyst and PMS in the system was limited, resulting in a limited quantity of active species being generated. Excessive NOR will compete for the limited active species, consequently leading to decreased removal efficiency.

**3.3.5. Effect of initial pH.** Different initial pH values will have an impact on the existence form of PMS and the activity of free radicals, and thus affect the degradation effect of NOR. In Fig. 6e, the NOR removal rates were similar when the pH was in the range of 5–8, and the removal rates within 6 min decreased to 84.4% and 94.1% at pH 4 and 9, respectively. Possible reasons of the decreased removal rates at pH 4 and 9 were as follows. Under acidic conditions, H<sup>+</sup> combines with the –O–O– bonds in PMS to form hydrogen bonds, which subsequently inhibited the generation of ·OH and SO<sub>4</sub>·<sup>-</sup> radicals, ultimately reducing NOR removal efficiency.<sup>42,43</sup> Since the pK<sub>a</sub> of PMS was 9.4, one of the main existing forms of PMS at pH 9 was SO<sub>5</sub><sup>2-</sup>, which may undergo decomposition through non-radical pathways.<sup>44,45</sup> In the initial pH range from 4 to 9, all the NOR removal rates were higher than 80%, indicating that the S/CoFeAl-LDH/PMS had a good NOR removal effect within a wide range.

**3.3.6. Effect of inorganic anions.** The inorganic ions existing in the system may have an impact on the degradation of pollutants. Therefore, several common inorganic anions in water (SO<sub>4</sub><sup>2-</sup>, Cl<sup>-</sup>, NO<sub>3</sub><sup>-</sup>, HCO<sub>3</sub><sup>-</sup>) were selected to explore their effects on the degradation of NOR *via* PMS activated by S/CoFeAl-LDH. As shown in Fig. 6f, after adding 5 mM HCO<sub>3</sub><sup>-</sup> to the solution, the removal rate of NOR decreased to 43.5%. This is because the CO<sub>3</sub><sup>·-</sup> generated from the reaction of HCO<sub>3</sub><sup>-</sup> with SO<sub>4</sub>·<sup>-</sup> in the solution has lower reactivity (eqn (1) and (2)), meaning that HCO<sub>3</sub><sup>-</sup> in water will inhibit the degradation of NOR.<sup>46,47</sup> In addition, when adding SO<sub>4</sub><sup>2-</sup>, Cl<sup>-</sup> and NO<sub>3</sub><sup>-</sup> to the solution, there was no significant change in the degradation rate of NOR within 6 min, proving that SO<sub>4</sub><sup>2-</sup>, Cl<sup>-</sup> and NO<sub>3</sub><sup>-</sup> in water will not have a significant impact on the activation of PMS by S/CoFeAl-LDH.



### 3.4. Practical application, universality and reusability of catalyst

The degradation of NOR in actual water samples by the S/CoFeAl-LDH/PMS system was investigated to explore the practical application of the proposed method (Fig. 7a). When 20 mg per L NOR was added to the filtered Pearl River water, the removal rate of NOR within 6 min was 71.1%. This is because the composition of the Pearl River water was relatively complex, where the contained ions and organic matter could influence the activation of PMS by S/CoFeAl-LDH, thereby affecting the

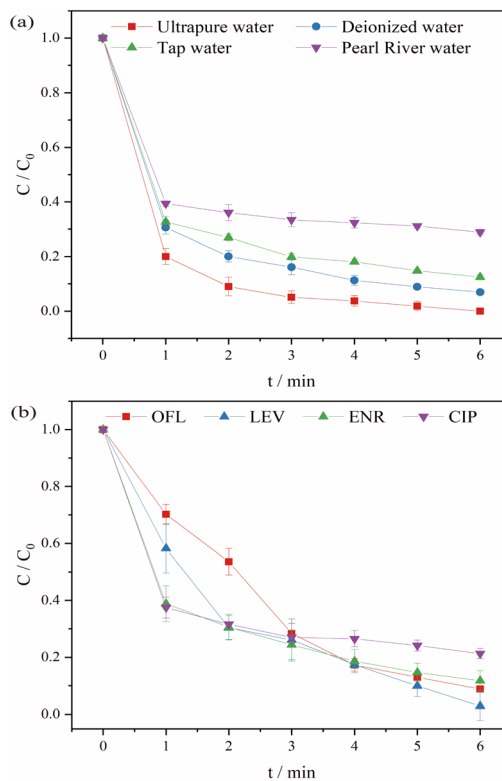


Fig. 7 Removal of NOR in different water samples (a) and Removal of different antibiotics (b) by the S/CoFeAl-LDH/PMS system. Reaction conditions:  $c_{\text{catalyst}} = 0.1 \text{ g L}^{-1}$ ,  $c_{\text{PMS}} = 0.2 \text{ g L}^{-1}$ , initial pH = 6.8,  $c_{\text{NOR}} = c_{\text{OFL}} = c_{\text{LEV}} = c_{\text{ENR}} = c_{\text{CIP}} = 20 \text{ mg L}^{-1}$ .

generation of free radicals and inhibiting the degradation of NOR. Nevertheless, a relatively high removal rate could still be achieved within 6 min. The removal rate within 6 min in tap water was 87.5%, which was slightly lower than that in deionized water and ultrapure water. The composition of the treated tap water was not as complex as that of the Pearl River water, but various ions and organic substances in the water had not been completely removed, which would have a certain impact on the degradation of NOR.

Furthermore, in order to evaluate the universality of the S/CoFeAl-LDH/PMS system, other quinolone organic compounds including ofloxacin (OFL), levofloxacin (LEV), enrofloxacin (ENR), and ciprofloxacin (CIP) were used as target pollutants. The S/CoFeAl-LDH/PMS system removed 78.7% CIP, 88.2% ENR, 91.2% OFL and 97.1% LEV within 6 min (Fig. 7b), indicating that the S/CoFeAl-LDH/PMS exhibited universal applications for the degradation removal of quinolone antibiotics.

For investigating the reusability of the S/CoFeAl-LDH material, the S/CoFeAl-LDH after the reaction was collected by a magnet and repeatability test was conducted under the same experimental conditions. For four cycles of experiments, the NOR removal rates within 6 min were 98.3%, 96.7%, 92.2% and 84.3%, respectively (Fig. S6). The experimental results showed that the S/CoFeAl-LDH still had a good NOR degradation effect after multiple uses.



The performance of the S/CoFeAl-LDH for NOR degradation was compared with other PMS activators (such as transition metal catalysts and carbon-based catalysts), with the results shown in Table S1. It can be observed that this S/CoFeAl-LDH material exhibited high catalytic activity, requiring a relatively low catalyst dosage ( $0.1 \text{ g L}^{-1}$ ) for NOR degradation, which helped reduce metal leaching pollution. Meanwhile, a lower PMS dosage ( $0.2 \text{ g L}^{-1}$ ) and the elimination of the need for pH adjustment reduced overall operational costs. It possessed strong magnetic properties, facilitating post-application recovery and reuse, thereby reducing catalyst production demands and saving costs. Moreover, it demonstrated efficient and rapid NOR degradation capability, achieving a 98.3% degradation rate within 6 min, significantly reducing time cost. These results indicated that this system held great promise for applications in NOR degradation.

### 3.5. Degradation mechanism

In the process of activating PMS based on transition metals, the degradation process can be divided into free radical and non-free radical pathways. The free radical pathway mainly involved the generated reactive species ( $\cdot\text{OH}$ ,  $\text{SO}_4^{\cdot-}$  and  $\text{O}_2^{\cdot-}$ ) reacting with organic pollutants.<sup>48,49</sup> The non-radical pathway mainly relied on the production of  $^1\text{O}_2$  and electron transfer between PMS and organic pollutants.<sup>50,51</sup> The active species in the S/CoFeAl-LDH/PMS system were determined through quenching experiments by adding different free radical quenchers.

Methanol (MeOH), *tert*-butanol (TBA), *p*-benzoquinone (*p*-BQ), and furfuryl alcohol (FFA) were selected as the quenchers for  $\text{SO}_4^{\cdot-}$ ,  $\cdot\text{OH}$ ,  $\text{O}_2^{\cdot-}$  and  $^1\text{O}_2$ , respectively.<sup>52-54</sup> MeOH could

quench both  $\cdot\text{OH}$  and  $\text{SO}_4^{\cdot-}$ , while TBA showed higher sensitivity toward  $\cdot\text{OH}$ . As shown in Fig. 8a, after the addition of 0.5 M MeOH and 0.5 M TBA, the removal rates of NOR within 6 min decreased by 1.5% and 34.5%, respectively, indicating that the  $\text{SO}_4^{\cdot-}$  produced after activation played a significant role in the degradation of NOR. When 5 mM of *p*-BQ was added as the  $\text{O}_2^{\cdot-}$  quench agent, the NOR removal rate dropped from 98.3% to 62.6%, confirming the involvement of  $\text{O}_2^{\cdot-}$  in the degradation process.<sup>55</sup> After quenching  $^1\text{O}_2$  with FFA, the NOR removal rate was 66.8%. The above experiments illustrated that in the S/CoFeAl-LDH/PMS system for NOR degradation,  $\text{SO}_4^{\cdot-}$ ,  $\text{O}_2^{\cdot-}$  and  $^1\text{O}_2$  all participated in the degradation process.

Based on the quenching experiment, EPR technology was further utilized to identify the active species in the system. The specific operation steps were described in Text S4. In Fig. 8b, no characteristic signals were observed in the PMS/DMPO system, indicating that PMS itself did not generate free radicals. However, weaker signals could be observed in the presence of S/CoFeAl-LDH, indicating that a small amount of  $\cdot\text{OH}$  and  $\text{SO}_4^{\cdot-}$  were generated in the S/CoFeAl-LDH/PMS system. As can be seen from Fig. 8c, the S/CoFeAl-LDH/PMS/DMPO system exhibited a characteristic 1 : 1 : 1 : 1 signal peak corresponding to DMPO- $\text{O}_2^{\cdot-}$ , confirming the generation of  $\text{O}_2^{\cdot-}$  during the reaction. Furthermore, by adding TEMP as the trapping agent for  $^1\text{O}_2$ , distinct signal peaks with an intensity ratio of 1 : 1 : 1 could also be observed (Fig. 8d), proving the existence of a non-radical pathway in the degradation process.<sup>56</sup>

The electron transfer during the degradation process was investigated using chronoamperometry, with detailed experimental procedures provided in Text S3. As shown in Fig. S7, with the S/CoFeAl-LDH modified electrode as the working

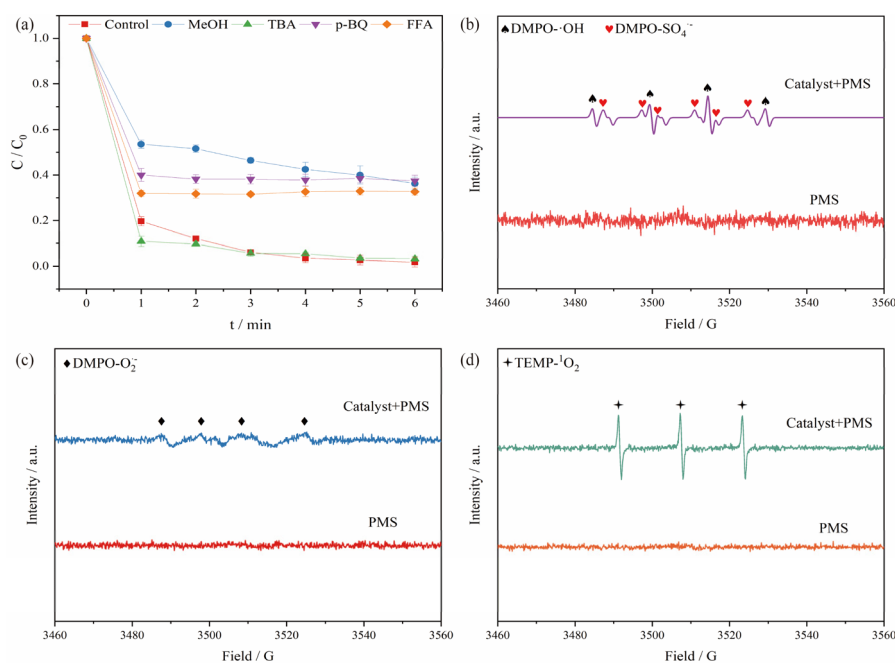


Fig. 8 Removal of NOR in the presence of different free radical quenchers (a); DMPO spin-trapping EPR spectra for  $\cdot\text{OH}$ ,  $\text{SO}_4^{\cdot-}$  and  $\text{O}_2^{\cdot-}$  respectively (b and c) and TEMP spin-trapping EPR spectra for  $^1\text{O}_2$  (d). Reaction conditions:  $c_{\text{catalyst}} = 0.1 \text{ g L}^{-1}$ ,  $c_{\text{PMS}} = 0.2 \text{ g L}^{-1}$ ,  $c_{\text{NOR}} = 20 \text{ mg L}^{-1}$ , initial pH = 6.8.

electrode, a significant current change was observed upon adding PMS to the solution, indicating electron transfer from the electrode to PMS.<sup>46</sup> Subsequent addition of NOR induced another distinct current variation, demonstrating electron transfer between the target pollutant and the electrode. The above electrochemical experiments confirmed the existence of an electron transfer pathway in the S/CoFeAl-LDH-activated PMS system for NOR degradation.

### 3.6. Structural characterization of catalyst after reaction

The valence state changes of S/CoFeAl-LDH elements before and after the reaction were characterized by XPS. The transition metals in LDH can activate PMS to produce active species. As shown in Fig. 9a, compared with the fresh catalyst, the content of Co<sup>2+</sup> decreased from 41.03% to 29.99%, and the content of Co<sup>3+</sup> increased from 58.97% to 70.01%. In Fig. 9b, the contents of Fe<sup>2+</sup> and Fe<sup>3+</sup> in the fresh S/CoFeAl-LDH were 32.98% and 67.02%, respectively. After the reaction, the Fe<sup>2+</sup> and Fe<sup>3+</sup> contents in the S/CoFeAl-LDH changed to 48.01% and 51.99%, respectively. The above proved that redox reactions occurred between PMS and both Co<sup>2+</sup>/Co<sup>3+</sup> and Fe<sup>2+</sup>/Fe<sup>3+</sup> (eqn (3)–(6)).<sup>34,57</sup> Generally, SO<sub>4</sub><sup>•-</sup>/SO<sub>5</sub><sup>•-</sup> was produced by the reaction between Co<sup>2+</sup>/Fe<sup>3+</sup> and PMS. The generated SO<sub>4</sub><sup>•-</sup>/SO<sub>5</sub><sup>•-</sup> can be converted into other ROS (•OH, <sup>1</sup>O<sub>2</sub>) through its own reaction or by reacting with H<sub>2</sub>O/OH<sup>-</sup>. The reaction equations for the generation of free radicals in the reaction was eqn (7)–(11).<sup>58,59</sup> In the material, metal ions in low valence states reacted with PMS to generate active species. Therefore, the content of low-valence

metal ions in the system affected the quantity of free radicals produced, thereby influencing the degradation efficiency. The redox potential of Co<sup>3+</sup>/Co<sup>2+</sup> is 1.83 V, while Fe<sup>3+</sup>/Fe<sup>2+</sup> is 0.77 V. Therefore, Fe<sup>2+</sup> in the material can reduce the generated Co<sup>3+</sup> back to Co<sup>2+</sup> (eqn (12)). The synergistic effect between the metals promoted the generation of low-valence cobalt ions, which facilitated the degradation of NOR. After the reaction, the content of Fe<sup>3+</sup> decreased. It was inferred that the reducing sulfur species introduced by sulfidation reduced some of the high-valent metal ions to low-valent metal ions. The S 2p XPS spectra (Fig. 9c) revealed that the content of SO<sub>x</sub> increased from 68.81% to 73.43%, while the content of M–S decreased from 31.19% to 26.57%, confirming that reduced sulfur species participated in the redox process (eqn (13)).<sup>60</sup> Sulfidation promoted the recycling and regeneration of low-valent metal ions, which was conducive to the activation of PMS to generate free radicals. Moreover, the peak area of M–OH in Fig. 9d decreased from 74.43% to 45.86%, indicating the consumption of M–OH during the process (eqn (14)).<sup>61</sup>

According to the above experiments and previous studies, the possible degradation mechanism of NOR in the S/CoFeAl-LDH/PMS system was shown in Fig. 10, and the mechanism of S/CoFeAl-LDH activating PMS was as follows:

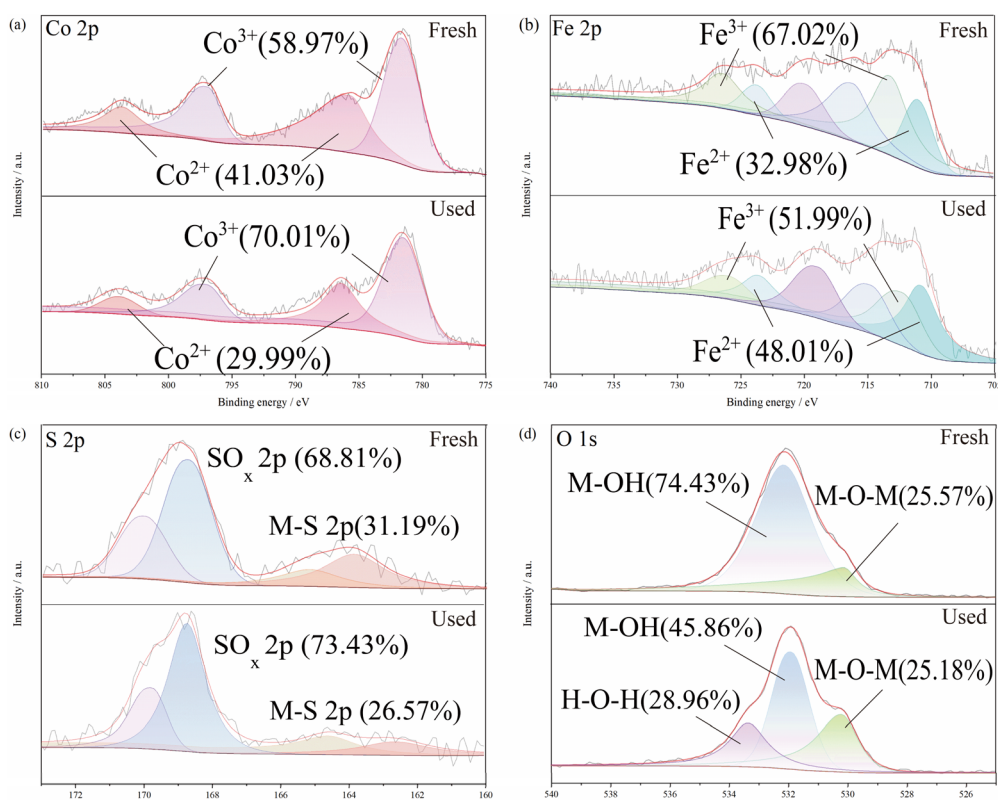
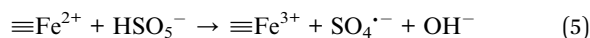
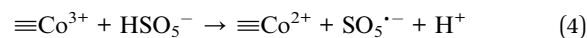
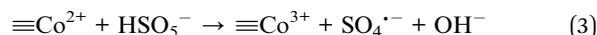
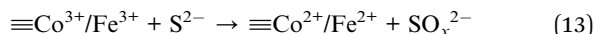
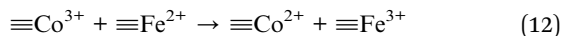
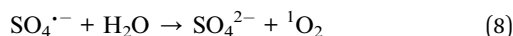
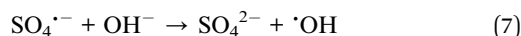
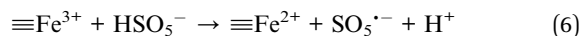


Fig. 9 XPS patterns of the fresh and the used S/CoFeAl-LDH: Co 2p (a), Fe 2p (b), S 2p (c) and O 1s (d).





### 3.7. Degradation pathway of NOR

Liquid chromatography-mass spectrometry (LC-MS) was used to identify the primary intermediate products of the degradation of NOR by S/CoFeAl-LDH activating PMS. During the degradation process, 15 intermediates were detected, and the results were shown in Fig. S8. Based on the experimental findings and relevant literature, the degradation pathways of NOR were proposed to occur through four main routes. The decomposition of NOR mainly occurred through processes such as the transformation of piperazine groups, the conversion of quinolone groups, decarboxylation and defluorination, as well as ring-opening. After further forming a series of small molecules, it was eventually mineralized into  $\text{CO}_2$  and  $\text{H}_2\text{O}$ .<sup>62–65</sup>

### 3.8. Biological toxicity of intermediates

The biological toxicity of NOR and the intermediates in the NOR degradation process was evaluated using ECOSAR (Fig. S9). The relevant data were summarized in Table S2. For acute toxicity,

most intermediates were harmless. P2, P6, P7 and P8 were only harmful to water fleas, while P3 was harmful to fish and toxic to water fleas and green algae. For chronic toxicity, P1, P4, P5, P10 and P11 were harmless, while some intermediates were toxic. To reduce the toxicity brought by intermediates, the degradation time can be further prolonged or the catalyst dosage can be increased, thereby increasing the degree of mineralization and reducing environmental pollution.

## 4. Conclusions

In this study, magnetic ternary CoFeAl-LDH was synthesized by the hydrothermal method, and sulfur-modified LDH (S/CoFeAl-LDH) was obtained using  $\text{Na}_2\text{S}$  as the sulfur source. The removal rate of NOR (initial concentration  $20 \text{ mg L}^{-1}$ ) by the S/CoFeAl-LDH/PMS system could reach 98.3% within 6 min. After 4 cycles, the degradation efficiency of NOR still reached 84.3%, indicating the good stability of the catalyst. The excellent catalytic performance was attributed to the reaction between low-valence metal ions and PMS. Besides, the synergistic effect between metals and the presence of sulfur species promoted the cyclic regeneration of low-valence metal ions. Finally, the oxidation and reduction between  $\text{Co}^{2+}/\text{Co}^{3+}$  and  $\text{Fe}^{2+}/\text{Fe}^{3+}$  contributed to the regeneration of  $\text{Co}^{2+}$ . Through quenching experiments and EPR experiments, the main active species in the reaction process were determined to be  $\text{SO}_4^{\cdot-}$ ,  $\text{O}_2^{\cdot-}$  and  ${}^1\text{O}_2$ . To sum up, the S/CoFeAl-LDH/PMS system can achieve highly efficient and rapid degradation of NOR, holding promising potential for the removal of organic pollutants from wastewater.

## Author contributions

X. Zhu: conceptualization, methodology, investigation, visualization, data curation, writing – original draft. X. Chen: conceptualization, methodology, validation. J. Wang: methodology, conceptualization. Caiyan Ge: methodology, conceptualization. M. Guo: resources, conceptualization, writing – review & editing, supervision, project administration, funding acquisition. Y. Cao: supervision, resources, writing – review & editing. B. Lin: supervision, resources.

## Conflicts of interest

There are no conflicts to declare.

## Data availability

All the data supporting this article have been included in the main text and its supplementary information (SI). Supplementary information is available. See DOI: <https://doi.org/10.1039/d5ra05588a>.

## Acknowledgements

This work was financially supported by the National Natural Science Foundation of China (No. 52070080).

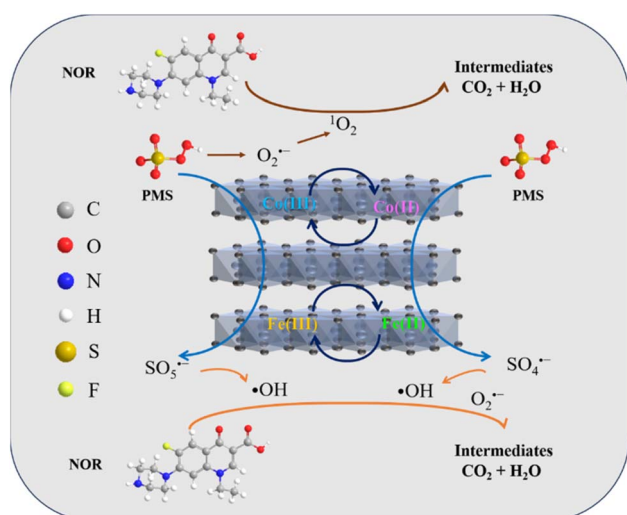


Fig. 10 Possible degradation mechanism of NOR in the S/CoFeAl-LDH/PMS.



## References

- H. Yu, D. Dou, X. Zhang, L. Zhang, H. Dong and H. Yu, *J. Cleaner Prod.*, 2020, **242**, 118548.
- C. Chen, X. Zhang, E. Liu, J. Xu, J. Sun and H. Shi, *J. Mater. Sci. Technol.*, 2024, **198**, 1–11.
- X. Yang, X. Zhang, Z. Wang, S. Li, J. Zhao, G. Liang and X. Xie, *Appl. Catal., B*, 2019, **255**, 117752.
- S. Kumari, A. A. Khan, A. Chowdhury, A. K. Bhakta, Z. Mekhalif and S. Hussain, *Colloids Surf., A*, 2020, **586**, 124264.
- A. S. Eltaweil, A. M. Abdelfatah, M. Hosny and M. Fawzy, *ACS Omega*, 2022, **7**, 8046–8059.
- M. A. T. Hussein, M. M. Motawea, M. M. Elsenety, S. M. El-Bahy and H. Gomaa, *Appl. Nanosci.*, 2022, **12**, 1519–1536.
- B. Zhou, Z. Yu, Q. Wei, H. Long, Y. Xie and Y. Wang, *Appl. Surf. Sci.*, 2016, **377**, 406–415.
- J. Ji, Y. Xu, H. Huang, M. He, S. Liu, G. Liu, R. Xie, Q. Feng, Y. Shu, Y. Zhan, R. Fang, X. Ye and D. Y. C. Leung, *Chem. Eng. J.*, 2017, **327**, 490–499.
- Y. Li, Q. Wang, X. Zhang, L. Dong, Y. Yuan, C. Peng, M. Zhang, P. Rao, Md. N. Pervez and N. Gao, *J. Water Process Eng.*, 2024, **57**, 104714.
- B. Xu, Z. Luo, T. Tao and Y. Wang, *Sep. Purif. Technol.*, 2024, **334**, 126321.
- T. Garoma, S. K. Umamaheshwar and A. Mumper, *Chemosphere*, 2010, **79**, 814–820.
- Y. Ding, L. Fu, X. Peng, M. Lei, C. Wang and J. Jiang, *Chem. Eng. J.*, 2022, **427**, 131776.
- L. Chen, X. Zuo, L. Zhou, Y. Huang, S. Yang, T. Cai and D. Ding, *Chem. Eng. J.*, 2018, **345**, 364–374.
- N. Li, J. Ye, H. Dai, P. Shao, L. Liang, L. Kong, B. Yan, G. Chen and X. Duan, *Water Res.*, 2023, **235**, 119926.
- S. Yang, P. Wang, X. Yang, L. Shan, W. Zhang, X. Shao and R. Niu, *J. Hazard. Mater.*, 2010, **179**, 552–558.
- Y. Wang, H. Li, J. Xu, J. Yu, J. Wang, H. Jiang, C. Li, X. Zhang and N. Liu, *Sep. Purif. Technol.*, 2024, **330**, 125399.
- Y. Hong, J. Peng, X. Zhao, Y. Yan, B. Lai and G. Yao, *Chem. Eng. J.*, 2019, **370**, 354–363.
- S. Wang and J. Wang, *Chem. Eng. J.*, 2019, **356**, 350–358.
- G. P. Anipsitakis and D. D. Dionysiou, *Environ. Sci. Technol.*, 2004, **38**, 3705–3712.
- S. Giannakis, K.-Y. A. Lin and F. Ghanbari, *Chem. Eng. J.*, 2021, **406**, 127083.
- N. Q. Tung, D. T. C. Van, D. X. Thang, N. T. K. An, T. T. Trang, B. D. Nhi, N. P. Thao, L. T. Son, N. N. Huy and N. T. Dung, *J. Environ. Chem. Eng.*, 2023, **11**, 110127.
- A. Jawad, Z. Liao, Z. Zhou, A. Khan, T. Wang, J. Ifthikar, A. Shahzad, Z. Chen and Z. Chen, *ACS Appl. Mater. Interfaces*, 2017, **9**, 28451–28463.
- J. Ali, L. Wenli, A. Shahzad, J. Ifthikar, G. G. Aregay, I. I. Shahib, Z. Elkhilifi, Z. Chen and Z. Chen, *Water Res.*, 2020, **181**, 115862.
- J. Wang, Z. Guo, F. Li, H. Yang, H. Che, Z. Zhang, Y. Wang, X. Zhang, S. Li and J. Mu, *J. Electroanal. Chem.*, 2023, **931**, 117189.
- X. Li, S. Xiong, X. Tang, R. Tang, Y. Deng and D. Gong, *J. Environ. Chem. Eng.*, 2024, **12**, 112483.
- H. Zeng, W. Zhang, L. Deng, J. Luo, S. Zhou, X. Liu, Y. Pei, Z. Shi and J. Crittenden, *J. Colloid Interface Sci.*, 2018, **515**, 92–100.
- X. Huang, M. Su, J. Zhou, W. Shu, Z. Huang, N. Gao and G. Qian, *Chem. Eng. J.*, 2017, **328**, 66–73.
- X. Huang, Q. Su, S. Han, J. Zhou, G. Qian and N. Gao, *J. Hazard. Mater.*, 2020, **389**, 122051.
- J. Rui, N. Deng, Y. Zhao, C. Tao, J. Zhou, Z. Zhao and X. Huang, *Chemosphere*, 2022, **302**, 134849.
- L. Yang, Y. Yue, R. Huang, W. Xiao, S. Wei and Z. Jiang, *Sep. Purif. Technol.*, 2024, **333**, 125821.
- Z. Zhu, J. Ye, X. Tang, Z. Chen, J. Yang, P. Huo, Y. H. Ng and J. Crittenden, *Environ. Sci. Technol.*, 2023, **57**, 16131–16140.
- Z. Yang, X. Tan and C. Zhang, *Sep. Purif. Technol.*, 2024, **336**, 126320.
- Y. Chen, L. Liu, J. Wei, Z. Liu, H. Wang, Y. Zhu, Q. Shao and P. Xie, *Chem. Eng. J.*, 2024, **492**, 152171.
- Z. Yang, X. Li, Y. Huang, Y. Chen, A. Wang, Y. Wang, C. Li, Z. Hu and K. Yan, *J. Cleaner Prod.*, 2021, **310**, 127584.
- S. Zhai, J. Liu, J. Sheng, J. Xu and H. Jiang, *Chem. Eng. J.*, 2021, **421**, 130403.
- M. Xu, J. Yang, Y. Wang, B. Lu, R. Chen and H. Liu, *Sep. Purif. Technol.*, 2022, **300**, 121822.
- J. Yang, M. Xu, P. Li and H. Liu, *Chemosphere*, 2024, **351**, 141207.
- T. Wu, W. Wang, J. Huang, X. Ren, X. Zhao and T. Zhou, *J. Saudi Chem. Soc.*, 2024, **28**, 101940.
- J. Wang, Z. Wang, N. Liu, C. Liu, J. Yan, C.-C. Li, J. Cui, J. Liu, X. Hu and Y. Wu, *J. Colloid Interface Sci.*, 2022, **615**, 173–183.
- H. Zeng, L. Deng, H. Zhang, C. Zhou and Z. Shi, *J. Hazard. Mater.*, 2020, **400**, 123297.
- J. Sheng, J. Xu, B. Qin and H. Jiang, *J. Environ. Manage.*, 2022, **310**, 114693.
- J. Song, X. Ren, G. Hu, X. Hu and W. Cheng, *Process Saf. Environ. Prot.*, 2023, **176**, 140–154.
- R. Wang, F. Chen, L. Gao, X. Ren and W. Guo, *J. Environ. Chem. Eng.*, 2022, **10**, 108361.
- X. Zhao, C. Niu, L. Zhang, H. Guo, X. Wen, C. Liang and G. Zeng, *Chemosphere*, 2018, **204**, 11–21.
- A. Rastogi, S. R. Al-Abed and D. D. Dionysiou, *Appl. Catal., B*, 2009, **85**, 171–179.
- Y. Yang, B. Jie, Y. Zhai, Y. Zeng, J. Kang, G. Cheng and X. Zhang, *J. Mol. Liq.*, 2024, **394**, 123723.
- R. Luo, C. Liu, J. Li, J. Wang, X. Hu, X. Sun, J. Shen, W. Han and L. Wang, *J. Hazard. Mater.*, 2017, **329**, 92–101.
- R. Tang, D. Gong, Y. Deng, S. Xiong, J. Deng, L. Li, Z. Zhou, J. Zheng, L. Su and L. Yang, *Chem. Eng. J.*, 2022, **427**, 131809.
- Y. Li, J. Bu, Y. Sun, Z. Huang, X. Zhu, S. Li, P. Chen, Y. Tang, G. He and S. Zhong, *Sep. Purif. Technol.*, 2025, **356**, 129945.
- E.-T. Yun, J. H. Lee, J. Kim, H.-D. Park and J. Lee, *Environ. Sci. Technol.*, 2018, **52**, 7032–7042.
- L. Tang, Y. Liu, J. Wang, G. Zeng, Y. Deng, H. Dong, H. Feng, J. Wang and B. Peng, *Appl. Catal., B*, 2018, **231**, 1–10.
- Y. Ji, C. Ferronato, A. Salvador, X. Yang and J.-M. Chovelon, *Sci. Total Environ.*, 2014, **472**, 800–808.



- 53 Y. Zou, W. Li, L. Yang, F. Xiao, G. An, Y. Wang and D. Wang, *Chem. Eng. J.*, 2019, **370**, 1286–1297.
- 54 Q. Zhang, D. He, X. Li, W. Feng, C. Lyu and Y. Zhang, *J. Hazard. Mater.*, 2020, **384**, 121350.
- 55 J. He, J. Huang, Z. Wang, Z. Liu, Y. Chen, R. Su, X. Ni, Y. Li, X. Xu, W. Zhou, B. Gao and Q. Li, *Chem. Eng. J.*, 2022, **439**, 135784.
- 56 X. Duan, H. Sun, Z. Shao and S. Wang, *Appl. Catal., B*, 2018, **224**, 973–982.
- 57 L. Hou, X. Li, Q. Yang, F. Chen, S. Wang, Y. Ma, Y. Wu, X. Zhu, X. Huang and D. Wang, *Sci. Total Environ.*, 2019, **663**, 453–464.
- 58 L. Zhou, C. Ferronato, J.-M. Chovelon, M. Sleiman and C. Richard, *Chem. Eng. J.*, 2017, **311**, 28–36.
- 59 J. Cao, S. Sun, X. Li, Z. Yang, W. Xiong, Y. Wu, M. Jia, Y. Zhou, C. Zhou and Y. Zhang, *Chem. Eng. J.*, 2020, **382**, 122802.
- 60 X. Wu, W. Zhao, Y. Huang and G. Zhang, *Chem. Eng. J.*, 2020, **381**, 122768.
- 61 X. Zhou, C. Luo, M. Luo, Q. Wang, J. Wang, Z. Liao, Z. Chen and Z. Chen, *Chem. Eng. J.*, 2020, **381**, 122587.
- 62 R. Su, L. Huang, N. Li, L. Li, B. Jin, W. Zhou, B. Gao, Q. Yue and Q. Li, *Chem. Eng. J.*, 2021, **414**, 128768.
- 63 N. S. Shah, J. A. Khanb, M. Sayedb, Z. U. H. Khana, A. D. Rizwana, N. Muhammada, G. Boczkajd, B. Murtazaa, M. Imrana, H. M. Khanb and G. Zamana, *Chem. Eng. J.*, 2018, **351**, 841–855.
- 64 Q. Wu, Y. Liu, H. Jing, H. Yu, Y. Lu, M. Huo and H. Huo, *Chem. Eng. J.*, 2020, **390**, 124615.
- 65 Z. Lin, Y. Wu, X. Jin, D. Liang, Y. Jin, S. Huang, Z. Wang, H. Liu, P. Chen, W. LV and G. Liu, *J. Hazard. Mater.*, 2023, **443**, 130195.

